

Article

Spatial and Temporal Variation of Aerosol and Water Vapour Effects on Solar Radiation in the Mediterranean Basin during the Last Two Decades

Maria A. Obregón ^{1,*}, Maria João Costa ², Ana Maria Silva ¹ and Antonio Serrano ³

¹ Department of Physics, Institute of Earth Sciences, Institute for Advanced Studies and Research, University of Évora, 7000-671 Évora, Portugal; asilva@uevora.pt

² Department of Physics, Institute of Earth Sciences, School of Science and Technology, University of Évora, 7000-671 Évora, Portugal; mjcosta@uevora.pt

³ Department of Physics, University of Extremadura, 06006 Badajoz, Spain; asp@unex.es

* Correspondence: nines@unex.es

Received: 27 March 2020; Accepted: 20 April 2020; Published: 22 April 2020



Abstract: This study aims to calculate and analyse the spatial and temporal variation of aerosol optical thickness (AOT) and precipitable water vapour (PWV) and their effects on solar radiation at the surface in the Mediterranean basin, one of the maritime areas with the largest aerosol loads in the world. For the achievement of this objective, a novel and validated methodology was applied. Satellite data, specifically CERES (Clouds and the Earth's Radiant Energy System) SYN1deg products during the period 2000–2018, were used. Results show that the spatial distribution of AOT and PWV are closely linked to the spatial distributions of its effects on solar radiation. These effects are negative, indicating a reduction of solar radiation reaching the surface due to aerosol and water vapour effects. This reduction ranges between 2% and 8% for AOT, 11.5% and 15% for PWV and 14% and 20% for the combined effect. The analysis of the temporal distribution has focused on the detection of trends from their anomalies. This study has contributed to a better understanding of AOT and PWV effects on solar radiation over the Mediterranean basin, one of the most climatically sensitive regions of the planet, and highlighted the importance of water vapour.

Keywords: radiative effects; aerosol optical depth; precipitable water vapour; Mediterranean basin; CERES

1. Introduction

Atmospheric aerosols and water vapour play an important role in the Earth's radiation balance, modifying the solar radiation that reaches the Earth's surface. When interacting with these atmospheric constituents, the solar radiation is affected by scattering and absorption processes. The effects of these constituents on the surface solar radiation are very important, affecting the diurnal and seasonal temperature variations (e.g., [1]), the surface energy balance (e.g., [2]), as well as the water cycle (e.g., [3]).

The Mediterranean basin, including the Mediterranean Sea and the surrounding land masses of Europe, Africa and Asia, is a very interesting region to analyse aerosol and water vapour effects on surface solar radiation. This interest is due to several reasons: the first and most important is that the Mediterranean basin is one of the regions most vulnerable to climate change [4]. This vulnerability is due to the fact that its meteorology is strongly influenced by the ocean-land interactions and by the complex orography, modifying the thermal regime and hydrological cycles. Another reason is that it is one of the sea areas with the highest aerosol load in the world [5]. In the Mediterranean basin, aerosols from different natural and anthropogenic sources converge and are mixed, such as mineral dust from

African and the Middle Eastern deserts, pollution from Europe and nearby coastal regions and marine aerosols [6]. This, together with the prolonged duration of sunlight and the small cloud cover in summer, produces large radiative effects. Several studies confirm that aerosol radiative effects during summer over the Mediterranean basin are among the highest in the world [7,8]. Another factor to be considered is the existence of an important source of water vapour in this region, the Mediterranean Sea, allowing for the study of the availability of water vapour over the Mediterranean basin and their radiative effects.

Due to great interest on the Mediterranean basin, several studies have analysed aerosols, water vapour and their effects on solar radiation in this area [9–18]. However, most of these studies are local (measurements taken at specific locations) or use a short period of study (specific campaigns), preventing a complete analysis of the spatial and temporal variability. Thus, only a few studies analyse the existence of trends in aerosols (e.g., [16]), water vapour (e.g., [19,20]) or their effects (e.g., [21]). The detection of long-term trends is of great interest because they help to understand the aerosol and water vapour cycles.

The main limitation of the existing studies comes from the fact that they examine the effect of aerosols (e.g., [9–14,17]) or water vapour (e.g., [15,18,22]) individually. Thus, to our knowledge, only the study by Obregón et al. [23] has analysed the joint effect of both atmospheric constituents and focuses on nine specific stations representative of different regions of the world. Studying the joint effect is of great interest since aerosols and water vapour are always present in the atmosphere, producing interactions between them that are masked if considered individually.

In this study, we propose to extend this methodology to a wide area such as the Mediterranean basin. For this purpose, data from CERES (Cloud and Earth Radiant Energy System) satellites have been used. Satellites provide long-term data records with a large spatial coverage, being the ideal source of information for this type of studies. They have already been used to monitor aerosols [17,24] and water vapour [25] in the Mediterranean basin but, as mentioned above, none of the previous studies have analysed the combined effect of both components.

Therefore, the present study aims to calculate and analyse the spatial and temporal variation of aerosols and water vapour and their combined effect on solar irradiation at ground level in the Mediterranean basin. In addition, the individual effects of aerosols and water vapour were calculated for comparison purposes. In contrast to previous existing studies, mainly focused on short campaigns and specific locations, this is, to our knowledge, the first study that analyses the combined effect of aerosols and water vapour in a wide area for a long period. In fact, the study period extends along 19 years (from 2000 to 2018), using one of the longest remote sensing derived climate data sets in the region, with the advantage of covering a wide area that is also considered one of the regions in the world most sensitive to climate change. Other authors have used shorter time series to evaluate AOD and PWV trends [26,27]. It is also the first study to apply a new methodology (which has been successfully tested on nine specific stations previously [23]) to a wide area, taking advantage of the extensive coverage provided by satellites. The long period and the wide area allow this study to perform a complete and significant analysis of the spatial and temporal variability of the area. The interest is enhanced by its application to the Mediterranean basin. As mentioned before, this area is of high importance due to its large vulnerability to climate change and because of being one of the sea areas with the highest aerosol load in the world.

The paper is structured as follows: The dataset and the methodology are presented in Section 2, the obtained results are discussed in Section 3, and the conclusions are summarized in Section 4.

2. Dataset and Methodology

The aim of this study is to calculate and analyse the effect of aerosols and water vapour on solar irradiance at ground level in the Mediterranean basin. For that purpose, the methodology recently developed by Obregón et al. [23] has been used in this study. This methodology, which was successfully validated at nine stations representative for different regions in the world [23], is here applied to a wide area such as the Mediterranean basin using satellite data. According to it, aerosols are characterized by the aerosol optical thickness (AOT) and water vapour by the integrated water vapour (PWV). AOT is representative for the aerosol load in the atmospheric column. Specifically, AOT at 550 nm has been used since it is a reference wavelength extensively used (e.g., [28,29]), therefore convenient for comparison purposes. PWV is the column integrated amount of water vapour. AOT and PWV data used in this study have been obtained from satellite-based instruments, offering an unprecedented opportunity since they provide data with a global coverage. In this framework, CERES (Clouds and the Earth's Radiant Energy System) provides long-term global estimates of the radiative fluxes within the Earth's atmosphere and consistent cloud and aerosol estimates. Specifically, CERES SYN 1deg [30–32] daily AOT at 550 nm and PWV products, version Ed4A, have been used to calculate aerosol and water vapour effects. The "1deg" stands for 1-degree spatial resolution. The temporal resolution used is daily. The SYN1deg product combines Terra and Aqua CERES and MODIS observations, and 3-hourly geostationary (GEO) data. In particular, aerosol data comes from the NASA/GSFC MODIS MOD04_L2/MYD04_L2 products [33] as assimilated by MATCH Aerosol Transport Model constituents [34]. These MODIS retrievals consist of two readings (1030 and 1330 local time on Terra and Aqua, respectively) at 1-degree resolution. The dataset used was composed of 6880 daily CERES values of AOT and PWV, corresponding to the available period from March 1, 2000 to December 31, 2018. It should be mentioned that the stable anticyclonic weather conditions in the Mediterranean region facilitate the availability of long periods with continuous measurements, especially in summer. The uncertainty on AOT is $\pm 0.03 \pm 0.05 \cdot \text{AOT}$ over ocean and $\pm 0.05 \pm 0.15 \cdot \text{AOT}$ over land [33]. The uncertainty on PWV ranges between 5% and 10% [35]. MODIS retrievals of AOT have been thoroughly validated by comparison to AERONET (Aerosol Robotic Network) data worldwide. For instance, Sayer et al. [36] compare Deep Blue Collection 6 AOT at 550 nm from MODIS Aqua against AERONET data from 60 sites worldwide, obtaining a good correlation between the two datasets, with $R = 0.92$. Chu et al. [37] made an extensive validation of MODIS and AERONET data encompassing 315 co-located AOT from more than 30 AERONET sites, finding retrieval errors of $\Delta \text{AOT} = \pm 0.05 \pm 0.2 \text{ AOT}$. Moreover, Remer et al. [33] made an extensive validation effort with over 8000 MODIS retrievals collocated with AERONET measurements of AOT. They concluded that, globally, MODIS products are accurate to within prelaunch expectations, namely, $\pm 0.05 \pm 0.15 \text{ AOT}$ over land and $\pm 0.03 \pm 0.05 \text{ AOT}$ over ocean. Regarding our area of study, Mishra et al. [38] compared AOT from MODIS and AERONET at 15 sites around the Mediterranean basin and obtained a strong spatial agreement and relatively low biases of model AOT against MODIS observations, with moderate to high correlations ($R > 0.5$) around each site up to ~200–500 km radius. With regard to PWV, Prasad et al. [39] found that MODIS NIR clear column ($R^2 = 0.97$, RMSE = 5.44 mm) and IR ($R^2 = 0.81$, RMSE = 7.17 mm) water vapour show similar performance on comparison with AERONET data.

Obregón et al. [23] estimated the effect of AOT and PWV on solar radiation at the surface as a function of the AOT and PWV values. Following that methodology, downwelling shortwave (SW) irradiances under cloud-free conditions were simulated using the libRadtran (Version 1.7) radiative transfer model for each of 100 combinations consisting of pairs of selected values for AOT (between 0 and 1.5) and for PWV (between 0 and 60 mm). Thus, the individual effect of AOT or PWV was estimated as the variation in SW irradiance caused by a change in one variable (AOT or PWV) while the other one remains fixed. This variation is quantified by the relative difference (Rel.Dif), expressed as

percentages, and calculated with respect to an atmosphere with AOT = 0 or PWV = 0. The expression used to calculate the individual effect of AOT is [23]:

$$\text{Rel.Dif.}(AOT) = 100 \% * (I(AOT, PWV) - I_{\text{ref}}(0, PWV)) / I_{\text{ref}}(0, PWV) \quad (1)$$

where I is the simulated SW irradiance for each AOT value, and I_{ref} is the simulated SW irradiance for AOT equal to 0, while PWV value remains fixed. This calculation is done for every AOT value, obtaining at look-up table of Rel. Dif. for the individual effect of AOT (Table 1).

Similarly, the expression for the PWV effect is:

$$\text{Rel.Dif.}(PWV) = 100 \% * (I(AOT, PWV) - I_{\text{ref}}(AOT, 0)) / I_{\text{ref}}(AOT, 0) \quad (2)$$

where I is the simulated SW irradiance for each PWV value, and I_{ref} is the simulated SW irradiance for PWV equal to 0, while now it is AOT which remains fixed. This calculation is done for every PWV value, obtaining the look-up table of Rel. Dif. for the individual effect of PWV (Table 2).

The calculation of the combined effect of AOT and PWV follows the same methodology, but now both variables (AOT and PWV) can vary:

$$\text{Rel.Dif} = 100 \% * (I(AOT, PWV) - I_{\text{ref}}(0, 0)) / I_{\text{ref}}(0, 0) \quad (3)$$

where I is the simulated SW irradiance for any combination of AOT and PWV, and I_{ref} is the simulated SW irradiance for AOT and PWV equal to 0. The look-up table of Rel. Dif. for the combined effect of AOT and PWV calculated by Equation (3) is shown in Table 3.

Once the three look-up-tables have been computed, they are applied to AOT and PWV values provided by CERES product in order to obtain the effect on the SW irradiance of AOT and PWV individually, and combined. Thus, the daily relative differences (Rel.Dif(AOT), Rel.Dif(PWV) and Rel.Dif(AOT-PWV)) for each pixel of the Mediterranean basin were calculated. The bilinear interpolation method was used to obtain the intermediate value between the existing values in the look-up-tables. Subsequently, the spatial and temporal variability of these effects has been analysed. Temporal analysis was performed using a trend analysis to determine if AOT, PWV, AOT effects, PWV effects or AOT-PWV effects over time are increasing, decreasing or remaining the same. For this purpose, the Mann–Kendall Trend Test was used. This non-parametric test has the advantage of assuming no specific statistical distribution of the data. The application of the Mann–Kendall Trend test allows estimating the statistical significance of the trend. To determine the magnitude of the trend, Sen's method was used [40]. Before applying this test, the data has been deseasonalized in order to remove the large influence of the annual cycle, obtaining time series of AOT, PWV, AOT effects, PWV effects or AOT-PWV effects for each grid cell. The monthly anomaly is defined as the difference between the value for a certain month and the mean over the whole period of study for that month.

Obregón et al., 2018 [23] validated the methodology based on irradiance measurements in nine stations. The results obtained showed differences lower than 3% in 84% of the cases. The sensitivity of the model to different input variables of the model, as the aerosol and atmospheric vertical profiles and the surface albedo, was also calculated by Obregón et al. [23]. Rel.Dif values for different aerosol vertical profiles defined by the season and the aerosol type were calculated, obtaining maximum relative differences lower than 0.15%. When the aerosol type is considered, these relative differences are higher, but they do not exceed the value of 4.5%. This maximum relative difference was obtained due to the difference between urban and maritime aerosol types. A maximum relative difference of 0.24% was obtained when the sensitivity of Rel.Dif to the atmospheric profile was calculated. A maximum relative difference of 8.31% was obtained due to the variation of surface albedo between 0.05 and 0.8. These values guarantee the possibility of keeping the values of these variables fixed since they have no influence on the effect of aerosols and water vapour on radiation. These effects are modulated by the solar zenith angle.

Table 1. Relative difference values (%) describing the AOT effect on shortwave irradiance for each combination of aerosol optical thickness (AOT) and precipitable water vapour (PWV) values.

PWV (mm) AOT	0	6.66	13.33	20	26.66	33.33	40	46.66	53.33	60
0	0	0	0	0	0	0	0	0	0	0
0.16	-2.67	-2.93	-2.97	-2.99	-3.00	-2.95	-2.83	-2.72	-2.65	-2.64
0.33	-5.42	-5.91	-5.99	-6.02	-6.04	-5.91	-5.64	-5.38	-5.22	-5.18
0.50	-8.15	-8.84	-8.94	-8.99	-9.00	-8.78	-8.31	-7.89	-7.67	-7.65
0.66	-10.83	-11.70	-11.83	-11.89	-11.91	-11.59	-10.95	-10.38	-10.10	-10.09
0.83	-13.43	-14.48	-14.64	-14.71	-14.72	-14.33	-13.53	-12.83	-12.50	-12.50
1.00	-15.96	-17.17	-17.35	-17.43	-17.44	-16.98	-16.04	-15.22	-14.86	-14.86
1.16	-18.40	-19.76	-19.96	-20.05	-20.07	-19.54	-18.49	-17.56	-17.16	-17.17
1.33	-20.75	-22.25	-22.48	-22.58	-22.59	-22.01	-20.85	-19.83	-19.40	-19.42
1.5	-23.02	-24.65	-24.89	-25.00	-25.02	-24.40	-23.15	-22.05	-21.58	-21.60

Table 2. Relative difference values (%) describing the PWV effect on shortwave irradiance for each combination of AOT and PWV values.

PWV (mm) AOT	0	6.66	13.33	20	26.66	33.33	40	46.66	53.33	60
0	0	-10.25	-12.48	-13.96	-15.10	-16.04	-16.85	-17.56	-18.20	-18.78
0.16	0	-10.49	-12.75	-14.25	-15.40	-16.29	-16.99	-17.61	-18.18	-18.75
0.33	0	-10.71	-13.00	-14.51	-15.66	-16.48	-17.04	-17.53	-18.02	-18.58
0.50	0	-10.92	-13.24	-14.75	-15.89	-16.62	-17.00	-17.33	-17.77	-18.33
0.66	0	-11.12	-13.47	-14.99	-16.13	-16.76	-16.96	-17.15	-17.53	-18.11
0.83	0	-11.33	-13.70	-15.23	-16.37	-16.91	-16.94	-16.98	-17.32	-17.90
1.00	0	-11.53	-13.93	-15.47	-16.60	-17.06	-16.93	-16.83	-17.12	-17.71
1.16	0	-11.74	-14.16	-15.71	-16.84	-17.22	-16.94	-16.71	-16.95	-17.55
1.33	0	-11.94	-14.38	-15.94	-17.07	-17.38	-16.95	-16.60	-16.80	-17.41
1.5	0	-12.14	-14.61	-16.18	-17.31	-17.55	-16.98	-16.52	-16.66	-17.28

Table 3. Relative difference values (%) describing the AOT-PWV combined effect on shortwave irradiance for each combination of AOT and PWV values.

	0	6.66	13.33	20	26.66	33.33	40	46.66	53.33	60
0	0	-10.25	-12.48	-13.96	-15.10	-16.04	-16.85	-17.56	-18.20	-18.78
0.16	-2.67	-12.87	-15.08	-16.54	-17.66	-18.52	-19.21	-19.80	-20.36	-20.92
0.33	-5.42	-15.55	-17.72	-19.15	-20.23	-21.01	-21.54	-22.00	-22.46	-22.99
0.50	-8.15	-18.18	-20.31	-21.70	-22.75	-23.41	-23.76	-24.07	-24.47	-24.99
0.66	-10.83	-20.75	-22.84	-24.20	-25.21	-25.78	-25.96	-26.12	-26.46	-26.97
0.83	-13.43	-23.24	-25.29	-26.62	-27.60	-28.07	-28.10	-28.13	-28.43	-28.93
1.00	-15.96	-25.65	-27.67	-28.96	-29.91	-30.30	-30.19	-30.11	-30.35	-30.85
1.16	-18.40	-27.98	-29.95	-31.22	-32.14	-32.45	-32.22	-32.04	-32.23	-32.72
1.33	-20.75	-30.22	-32.15	-33.39	-34.28	-34.53	-34.19	-33.91	-34.07	-34.55
1.5	-23.02	-32.37	-34.27	-35.47	-36.35	-36.53	-36.10	-35.73	-35.85	-36.32

3. Results

3.1. Spatial Distribution

Figure 1a shows the spatial distribution of AOT averaged for the entire study period throughout the Mediterranean basin. AOT ranges between 0 and 0.45, with the highest values in North Africa and the lowest in the western part of the study region. In the rest of the study area, AOT does not differ much and ranges between 0.22 and 0.28, approximately. Specifically, the lowest AOT values, lower than 0.2, are located in the Iberian Peninsula and Southern France. The low value of aerosol load in this area is due to the influence of the Atlantic Ocean, a source of clean air masses (e.g., [41–44]). As mentioned, the highest AOT values are located in North Africa, due to the influence of one of the largest sources of aerosols: the Sahara Desert. Other areas with high AOT must also be noted such as,

for example, Bulgaria, specifically the area near Sofia, the capital of the country, where averaged AOT values higher than 0.30 are obtained. These high values were also described by Evgenieva et al. [45], who observed values in the range 0.22–0.41 for cloud-free skies. Another area with high AOT is the southwest of the study area, specifically the west of Middle East, where there is an important source of dust, Syria desert.

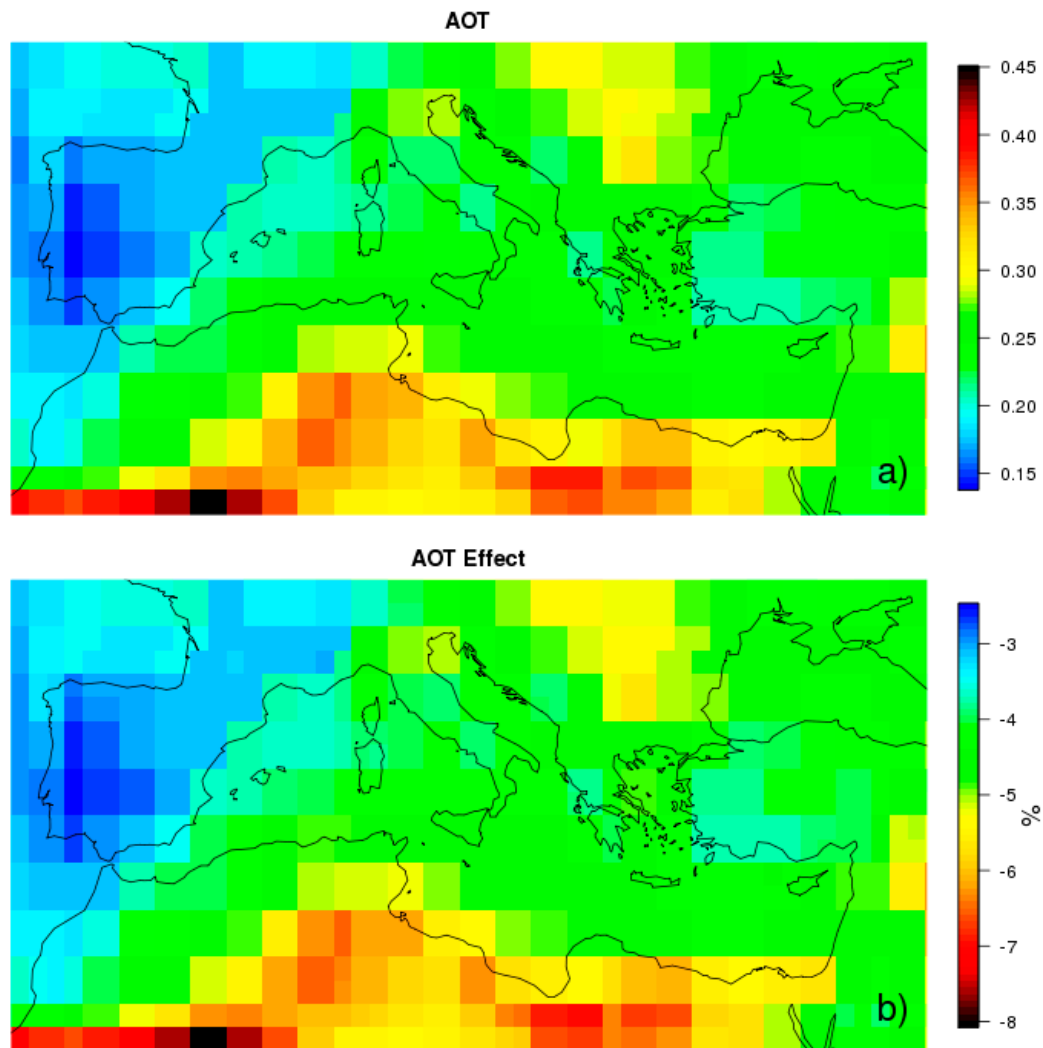


Figure 1. Distribution of averaged (a) AOT and (b) AOT effects on shortwave radiation at the surface over the Mediterranean basin during the period 2000–2018.

Regarding the effect of AOT on solar radiation, Figure 1b shows the spatial distribution of the relative difference as calculated by Equation (1). It shows the close similarity with the spatial distribution of AOT; the higher AOT, the higher effect on radiation. The highest effects are found over the deserts of North Africa and the west Middle East, and over the area around Bulgaria. Conversely, lower values are found over the Mediterranean Sea, specifically over the Iberian Peninsula and Southern France. These low AOT effects over the Iberian Peninsula and Southern France agree with those obtained by Papadimas et al. [46]. Another aspect to be noted is that AOT effect values for the entire study period are negative, indicating a reduction in the solar radiation reaching the surface due to the presence of aerosols. In fact, there is an average reduction in solar radiation between 2% and 8% for the entire study period.

When monthly-averaged values are analysed, the reduction in solar radiation reaches values higher than 10% in spring, with values above 12% in June (Figure 2). This figure shows the variability

existing during the year, with more negative values in April and June and less negative values from November to January. The analysis of the spatial distribution of the monthly-averaged AOT effects shows that the pattern during the cold months (November, December, January and February) is different from the rest of the year. During these cold months, the area with low effects on solar radiation expands from the Iberian Peninsula and Southern France into North Africa. This expansion is partly due to a decrease in the emission of dust by the Sahara in winter compared to summer [47]. On the other hand, it may be also connected to a greater abundance of absorbing aerosols emitted from heating systems and other anthropogenic activities in the cold season [42,48], which counterbalances the cooling effect of dispersive particles. During winter, Saharan dust is transported at low altitude [49] since the Intertropical Convergence Zone (ITCZ) is situated in its most southerly position and dust transport is controlled by high pressure systems located over North Africa [50].

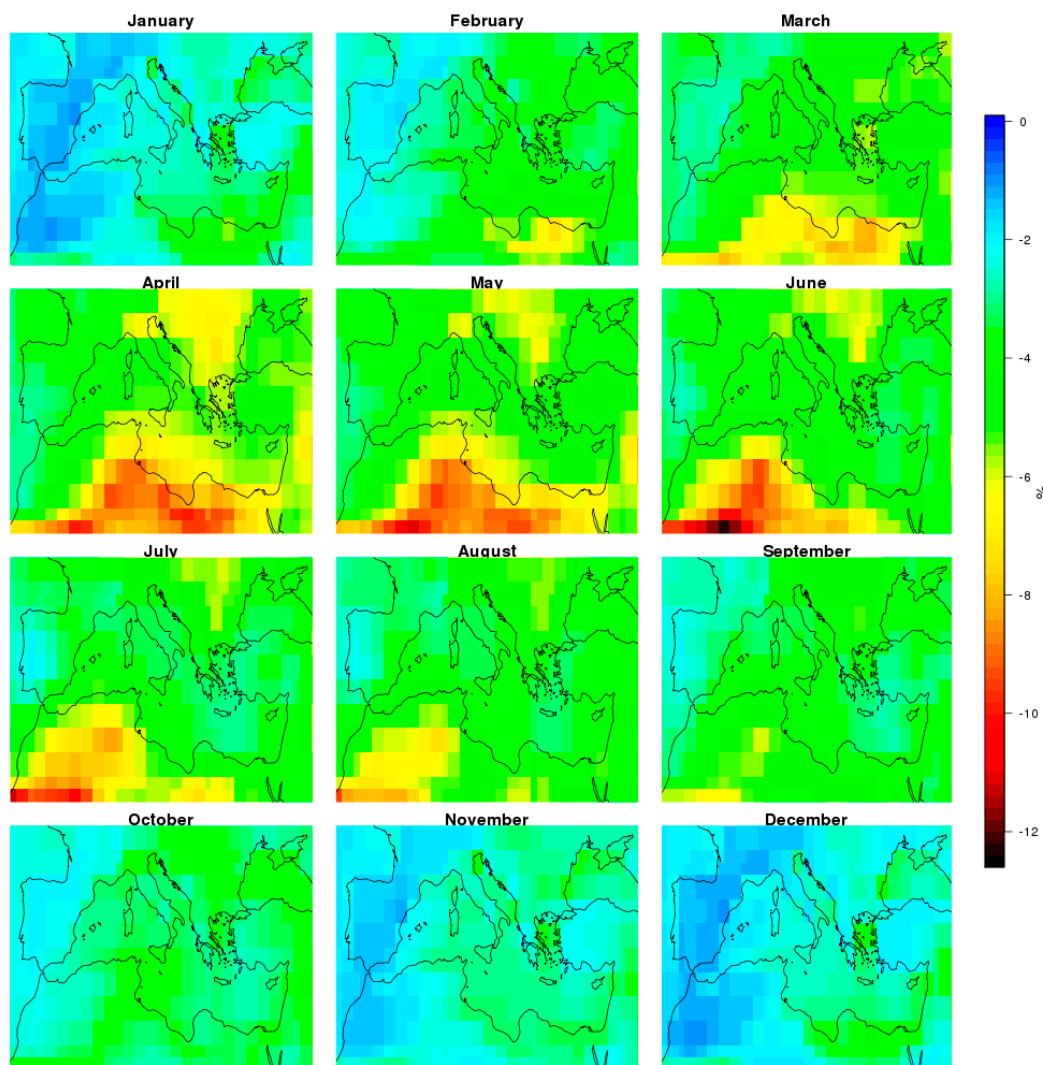


Figure 2. Distribution of monthly averaged AOT effects on shortwave radiation at the surface over the Mediterranean basin during the period 2000–2018. All figures have the same scale.

The spatial distribution of PWV is shown in Figure 3a. This figure shows that, as expected, the highest PWV values, around 20 mm, are obtained on water-covered surfaces since these constitute sources of moisture. Focusing on the Mediterranean Sea, it can be seen that the PWV over the western area is higher than over the eastern. The high values of monthly PWV during the summer contribute to this difference between the two regions (Figure 4). This behaviour has also been observed by

Palau et al. [51], and it can be attributed to the annual oscillation of the PWV in the eastern area, which does not follow the annual variation of solar irradiation and evaporation from the sea (with a maximum in summer and a minimum during winter season). Low PWV values during summer in the eastern region might occur because, during the summer months, advective conditions prevail in the mid-upper troposphere due to the Asian Monsoon system. This means higher ventilation conditions in the area with high rates of renewal of air masses aloft [52–54], while in the western area (under the influence of the Azores anticyclone) mesoscale vertical recirculation (low net ventilation conditions) is the most recurrent meteorological characteristic. However, as can be seen in Figure 4, during winter the behaviour is reversed, PWV in the eastern area is higher than in the western, although in both areas PWV is lower than in summer. This behaviour in PWV could be due to the fact that the western area is much more ventilated than in summer whereas in the eastern side, the extension of the Siberian Anticyclone system favours stagnation conditions in the troposphere [52,53]. High values of PWV and PWV effect are also observed in autumn on the coast of Libya and Tunisia. This increase can be related to the sensitivity of the hydrological system to land-use changes and, more recently, to air pollution effects as well. The combination of these effects may exceed critical threshold levels, e.g., the height of the cloud condensation levels with respect to the height of the coastal mountain ranges, resulting in the loss of summer storms [55]. The non-precipitated water vapour returns and accumulates over the sea. These changes and perturbations to the hydrological cycle involve an increase in Mediterranean cyclogenesis in autumn-winter through greenhouse heating of the sea surface by the water vapour and the pollutants accumulated over the sea.

As in the case of AOT, the spatial distribution of PWV is closely linked to the spatial distribution of its effects on solar radiation at the surface (Figure 3b). The higher the value of PWV, the greater its effect on radiation is. These effects are negative, indicating that water vapour reduces the solar radiation that reaches the surface. This reduction ranges between 11.5% and 15%, and therefore, it can be said that, in average, PWV effect is greater than AOT effect. As previously mentioned, the spatial distribution of PWV varies throughout the seasons, and therefore, its effects as well. Figure 5 shows the spatial distribution of PWV effect for different months of the year, obtaining more negative values in warm months and less negative values in cold months. Regardless of the month, the highest values of PWV effect occur over water surfaces. With regard to the lowest values of PWV effect, it should be noted that they are located over the Sahara and Syrian deserts, arid areas with low humidity, and in the Alps. The reason why PWV effect is so low over the Alps is that PWV generally decreases with increasing terrain altitude due to the decrease in temperature with height.

The combined effect of both atmospheric variables, AOT and PWV, has also been calculated. Figure 6c shows its average spatial distribution for the entire study period. As can be seen in this figure, AOT-PWV effect values are also negative, such as individual AOT and PWV effects, but the values are more negative, between -14% and -20% , while AOT is limited to range between -2% and -8% (Figure 6a) and PWV effect between -11.5% and -15% (Figure 6b). The analysis of the spatial distribution of AOT-PWV effect shows that the highest values occur over North Africa and southern Mediterranean Sea, coinciding with the areas with the greatest influence of aerosols and water vapour when considered individually. Conversely, the areas with the lowest effects are the Iberian Peninsula, Southern France, Alps and deserts of Sahara and Syria, which also coincide with the areas which showed the lowest influence of aerosol and water vapour when considered individually. This comparison between individual and combined effects emphasizes the importance of water vapour in reducing solar radiation at the surface that, however, has not been fully studied. Therefore, this study contributes to a better understanding of water vapour and its effects on solar radiation over the Mediterranean basin, one of the most climatically sensitive regions of the planet [56].

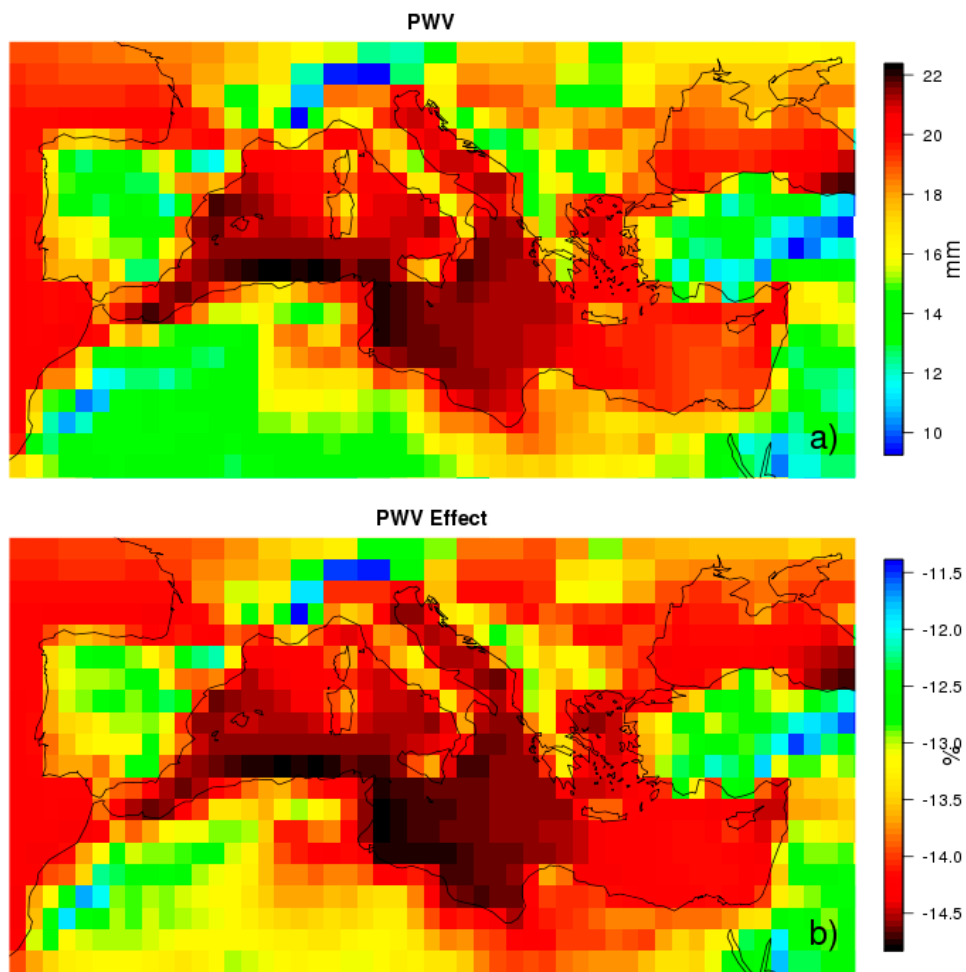


Figure 3. Distribution of averaged (a) PWV (mm) and (b) PWV effects on shortwave radiation at the surface over the Mediterranean basin during the period 2000–2018.

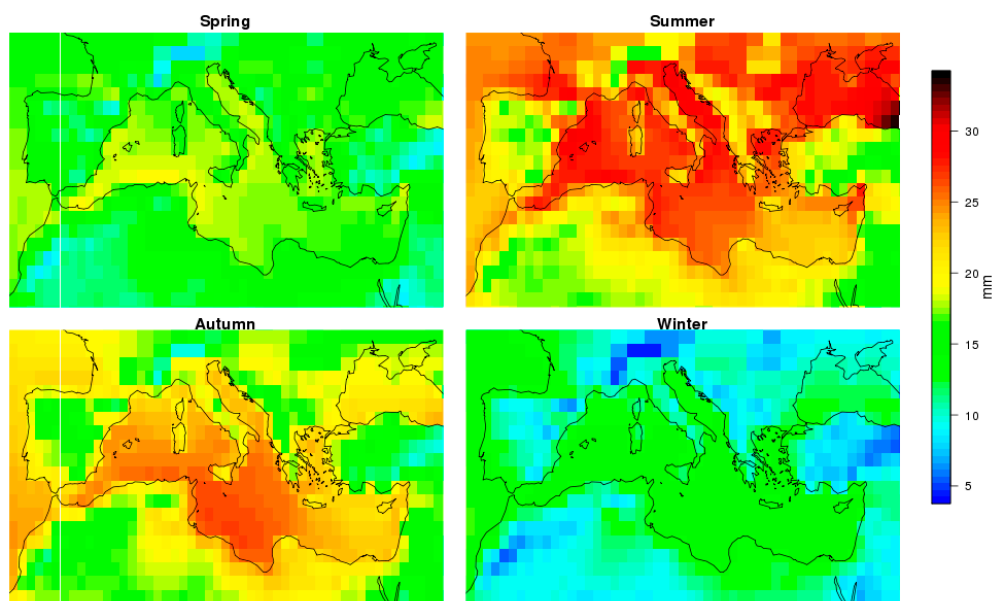


Figure 4. Distribution of seasonally averaged PWV in the Mediterranean basin during the period 2000–2018.

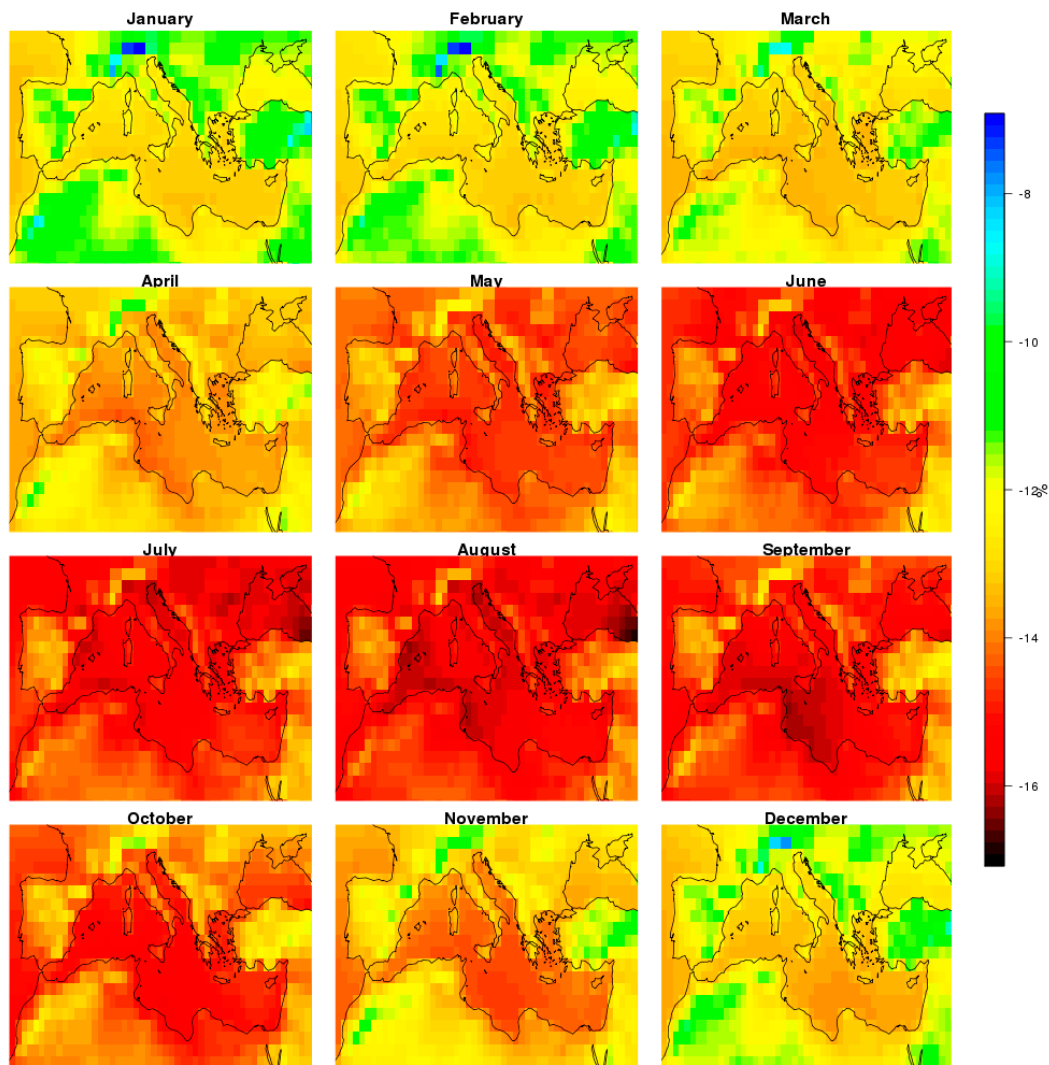


Figure 5. Distribution of monthly averaged PWV effects on shortwave radiation at the surface in the Mediterranean basin during the period 2000–2018. All figures have the same scale.

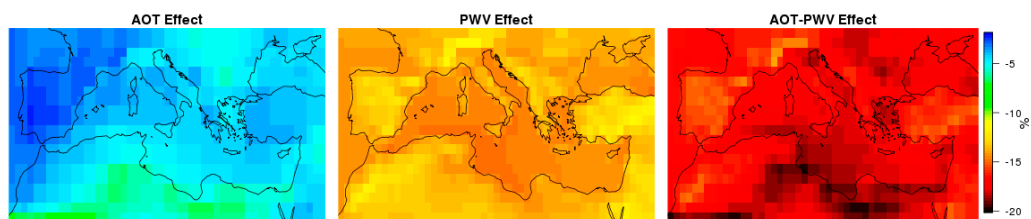


Figure 6. Distribution of averaged AOT effect, PWV effect and AOT-PWV effect on shortwave radiation at the surface over the Mediterranean basin during the period 2000–2018. All figures have the same scale.

3.2. Temporal Distribution

As already mentioned in the methodology section, the analysis of the temporal distribution of AOT, PWV and their effects on solar radiation at the surface has focused on the detection of trends from their anomalies. Figure 7 shows the monthly evolution of these anomalies. Figure 7a) shows that AOT decreases over the years, with a slope equal to -0.002 per year. This decrease is more pronounced since 2008, coinciding with the year that marked the beginning of the economic crisis that affected different

countries of the European community. This crisis caused a decline in the industrial production and in activities related to construction works, transport, etc., and consequently, a reduction in the emission of aerosols into the atmosphere (e.g., [48,57,58]). However, AOT values began to rise again in 2014, being probably related to an increase in industrial and transportation activities due to an increase in the country's real gross domestic product (GDP) growth rate with values of 0.9 in 2014 and 1.5 in 2015 [59]. The evolution of AOT effect (Figure 7c) shows the same pattern as AOT but with a positive slope of 0.038% per year. Since AOT effect values are negative, that positive trend indicates a decrease over time in the absolute value of the AOT effect. Unlike AOT, PWV increases throughout the study period with a positive slope equal to 0.055 mm per year (Figure 7b), and its effects decrease with a slope equal to -0.011% per year (Figure 7c), thus increasing its absolute value. This increase is in accordance with the forecast of Climate Change projections. According to Collins et al. [60]: "Annual surface evaporation is projected to increase as global temperatures rise over most of the ocean and is projected to change over land following a similar pattern as precipitation". Regarding the combined effect of AOT-PWV (Figure 7c), a trend equal to 0.019% per year is obtained for the entire study region. Since values of AOT-PWV effect are negative, this positive slope indicates a decrease in the absolute AOT-PWV effect throughout the study period.

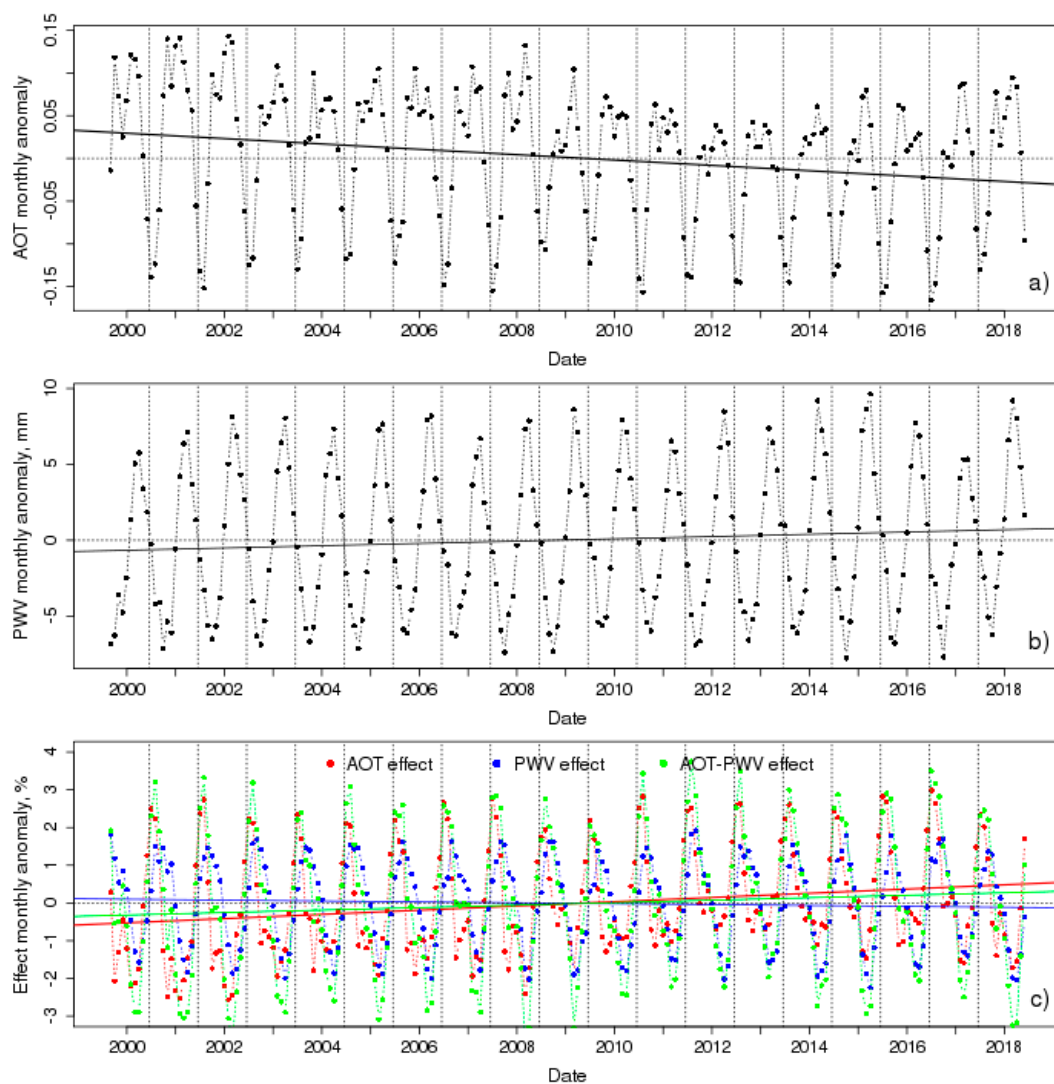


Figure 7. Evolution of monthly mean values of (a) AOT, (b) PWV, (c) AOT effect, PWV effect and AOT-PWV effect anomalies, for the Mediterranean basin, from March 2000 to December 2018. Straight lines are the linear fits for the monthly data.

Once analysed the temporal evolution of each constituent and its effects, their trends were calculated. For this, the Sen's method to determine the magnitude of the trend and the Mann-Kendall Trend test to estimate the statistical significance of the trend was used, as explained in the methodology. In the case of AOT, the trend is equal to -0.021 per decade during nearly 19 years, resulting in an absolute AOT decrease of 0.040. Statistically significant negative trends of AOT have also been obtained by other authors for the Mediterranean region (e.g., [17,61,62]). However, the values of these trends vary, depending on the study period considered. For example, the trend obtained by Zhang and Reid [61] is equal to -0.016 per decade, being its absolute value lower than the one obtained in our study. This may be due to the fact that their study period is 2000–2009, and the economic crisis had not greatly affected AOT values yet. On the contrary, trends obtained by Floutsi et al. [17] and Alfaro-Contreras et al. [62] show values of -0.030 and -0.023 per decade, respectively, being higher, in absolute terms, than that the one obtained in our study. This difference may be due to the fact that their study periods are 2002–2014 or 2002–2015, and therefore, the increase in AOT starting in 2014 has not been completely included. Figure 8 shows the spatial distribution of the linear trend in (a) AOT and (b) AOT effect, for 2000–2018 per decade. Pixels with levels of significance $p < 0.05$ are marked with a black dot. As shown in Figure 8a, AOT trends are negative throughout the study region, except in the west Middle East, where the intensity and frequency of dust storms has increased in recent years [63–65]. However, this positive trend is not significant. Most of the areas with significant trends are those with negative trends. As previously mentioned, AOT and AOT effect are closely related, so their spatial distributions are similar (Figure 8b). In the case of AOT effect, the trend is equal to 0.386% per decade during the period 2000–2019, resulting in an absolute AOT effect decrease of 0.728%.

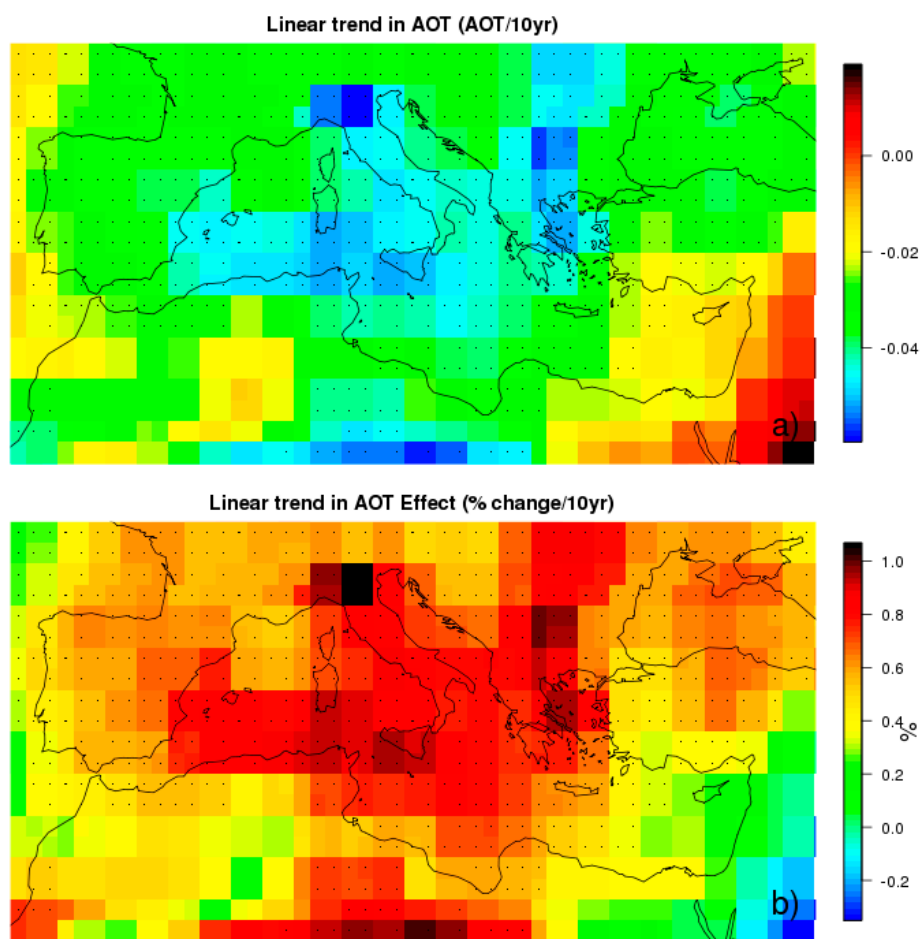


Figure 8. Spatial distribution of linear trend in (a) AOT and (b) AOT effect, for 2000–2018 per decade. Pixels with levels of significance $p < 0.05$ are marked with a black dot.

In the case of PWV, the trend is equal to 0.553 mm per decade during nearly 19 years, resulting in an absolute PWV increase of 1.042 mm. Statistically significant positive trends of PWV have also been obtained by other authors for the Mediterranean region for a similar period (e.g., [66,67]). However, if periods prior to that considered in this study are used, the PWV trend results negative (e.g., [19,68,69]). This fact highlights the importance of this study, because it remarks the importance of water vapour in recent years and its effects on solar radiation at the surface over the Mediterranean basin. Figure 9 shows the spatial distribution of linear trend in (a) PWV and (b) PWV effect for 2000–2018 per decade. Pixels with levels of significance $p < 0.05$ are marked with a black dot. As shown in Figure 9a, PWV trends are positive throughout the entire study region, although this increase in PWV values is only significant in regions of North Africa, specifically Algeria and Egypt. The highest trend values are obtained in the region of Romania and the Black Sea, while the lowest values, close to zero, are obtained in the south of the Iberian Peninsula. These low positive trend values are consistent with the results obtained by Mattar et al. [20], which obtained a negative trend in the south of the Iberian Peninsula and a positive one in the rest of Europe. In fact, southern Iberian Peninsula is the only region where positive trend values are obtained when analysing the spatial distribution of linear trends of PWV effect (Figure 9b). This figure shows that, in the rest of the study region, the trend values of PWV and PWV effect are closely related. It should be mentioned that the trend of PWV effect is not significant in any pixel. On average, the trend is equal to -0.115% per decade during the period 2000–2019 for the entire study region, resulting in an absolute PWV effect increase of 0.217%.

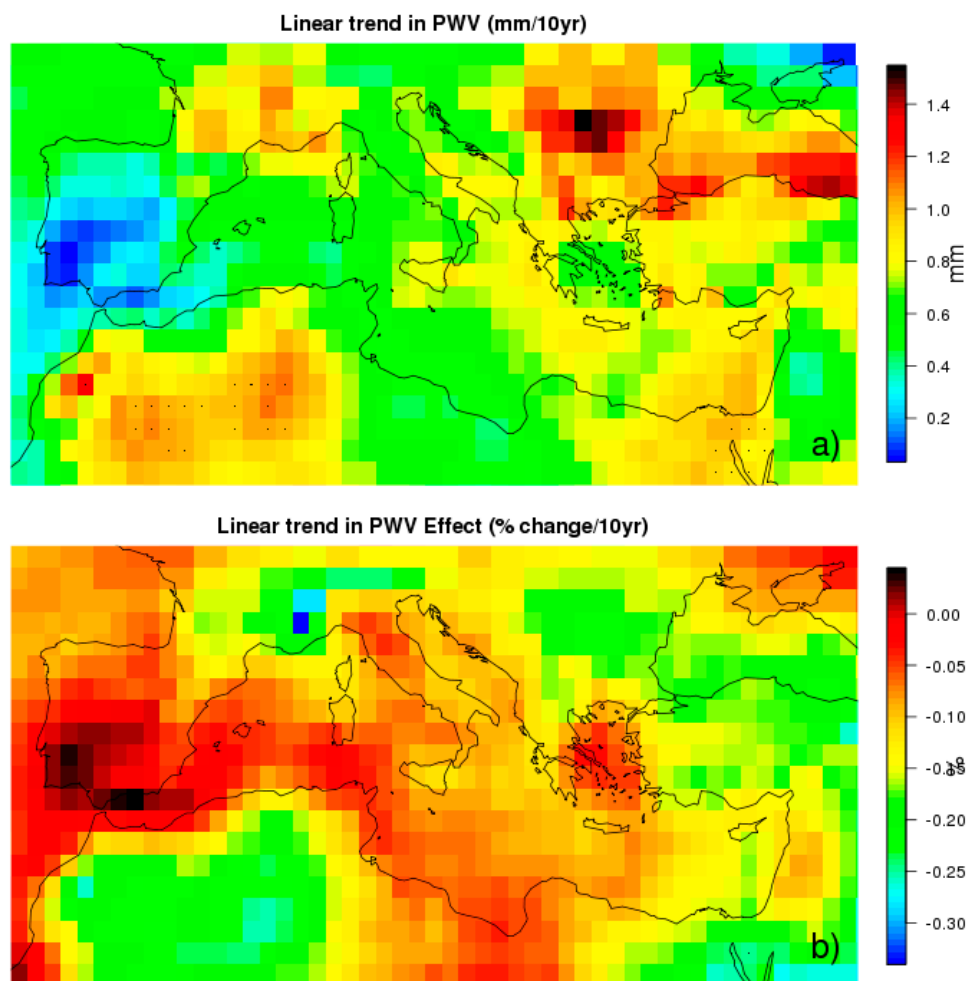


Figure 9. Spatial distribution of linear trend in (a) PWV and (b) PWV effect for 2000–2018 per decade. Pixels with levels of significance $p < 0.05$ are marked with a black dot.

The trend of the combined effect of AOT and PWV has also been calculated, obtaining a value equal to 0.195% per decade, which means that the effect decreases throughout the study period by 0.367%. These are the averaged values for the entire study region, but when their spatial distribution is analysed (Figure 10), the range of values is wider, specifically between -0.5 and 0.7 . This figure shows that the west Middle East is the only region where the trend is negative, and therefore, the effect increases throughout the study period due to the increase of the AOT effect, as shown in Figure 8. It is also found that the Iberian Peninsula, Italy and the Mediterranean Sea are the only regions where the trends are significant. In general, it is observed that the spatial distribution of the trend of AOT-PWV effect is similar to the trend of AOT effect, although the values are approximately half lower due to the influence of PWV effect, whose trend is opposite. Therefore, the combined analysis of aerosol and water vapour is suggested for trend studies focused on the Mediterranean basin, since they are two important atmospheric constituents in this region and have high effects on solar radiation at the surface.

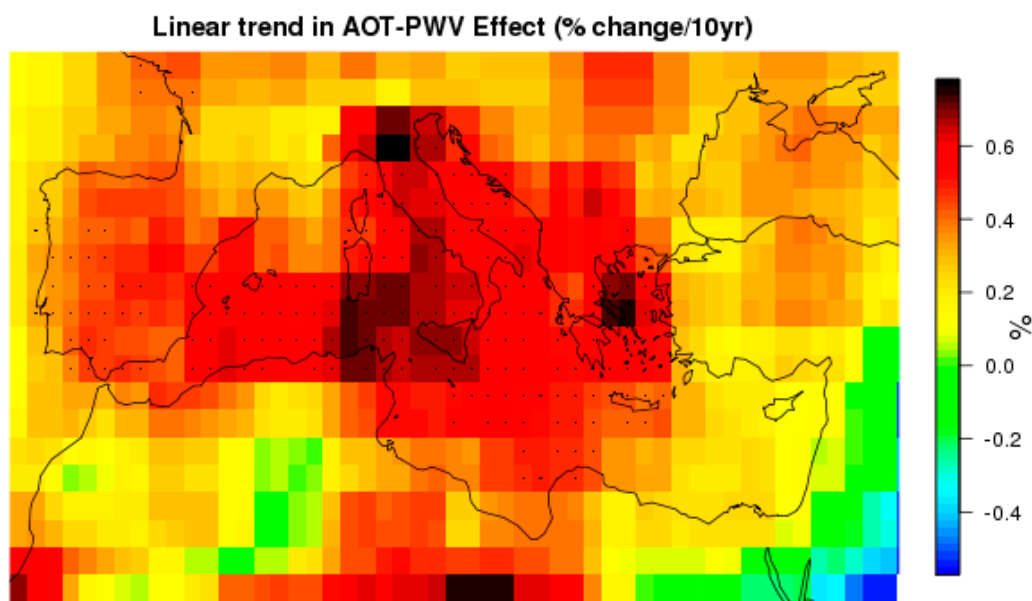


Figure 10. Spatial distribution of linear trend in AOT-PWV effect for 2000–2018 per decade. Pixels with levels of significance $p < 0.05$ are marked with a black dot.

4. Conclusions

In this study, the spatial and temporal variation of AOT and PWV and their effects on solar radiation at the surface in the Mediterranean basin have been calculated and analysed. This region is one of the most climatically sensitive regions of the planet due, among other things, to being one of the maritime areas with the largest aerosol load in the world and also to containing an important source of water vapour, the Mediterranean Sea. To solve the problem of spatial coverage limitation, satellite data, specifically CERES SYN1deg products, version Ed4A, have been used. The study period extends from 2000 to 2018. AOT effect, PWV effect and the combined effect of AOT and PWV have been calculated applying the novel and validated methodology proposed by Obregón et al. [23].

The results show that the spatial distributions of AOT and PWV are closely linked to the spatial distributions of their effects on solar radiation at the surface. The highest AOT values are located in North Africa, due to the influence of the Sahara Desert, while the lowest AOT values are located in the Iberian Peninsula and Southern France. In the case of PWV, the highest values are obtained over water-covered surfaces since these constitute sources of moisture. AOT effects and PWV effects are negative, indicating a reduction of solar radiation reaching the surface due to aerosol and water vapour effects. This reduction ranges between 2% and 8% for AOT and between 11.5% and 15% for PWV. Therefore, in average, PWV effect is greater than AOT effect. The combined effect of AOT and

PWV has also been calculated, obtaining also negative values, between 14% and 20%. The analysis of the spatial distribution of AOT-PWV effects shows that the highest effects occur over North Africa and southern Mediterranean Sea, coinciding with the areas with the greatest influence of aerosols and water vapour when considered individually.

The analysis of the temporal distribution has focused on the detection of trends from their anomalies. AOT trends are negative throughout the study region, except in the west Middle East. However, this positive trend is not significant. On average, the trend in AOT is equal to -0.021 per decade. This decrease in AOT values throughout the study period is also observed in AOT effect trend, whose value is equal to 0.386% per decade, resulting in an absolute AOT effect decrease of 0.728% . In the case of PWV, positive trend, equal to 0.553 mm per decade, is obtained. This increase in PWV values is only significant in regions of North Africa, specifically Algeria and Egypt. In regards to PWV effect, trend is not significant in any pixel. On average, PWV effect trend is equal to -0.115% per decade during the period 2000–2019 for the entire study region, resulting in an absolute PWV effect increase of 0.217% . The trend of AOT-PWV effect is 0.195% per decade, similar to the trend of AOT effect, although the values are approximately half lower due to the influence of PWV effect, whose trend is opposite.

This study has contributed to a better understanding of AOT and PWV effects on solar radiation over the Mediterranean basin, since they are two important atmospheric constituents in this region and have high effects on solar radiation at the surface. Therefore, the combined analysis of aerosol and water vapour is suggested in studies focused on the Mediterranean basin. The observational assessment of AOT and PWV effects on solar radiation in the Mediterranean basin is undoubtedly important for fields such as climate and land surface modelling where process understanding and model evaluation are crucial, as well as for energy meteorology, supporting for example the planning of future locations of solar power plants.

Author Contributions: Conceptualization, M.A.O., M.J.C., A.M.S. and A.S.; methodology, M.A.O., M.J.C., A.M.S. and A.S.; software, M.A.O., M.J.C., A.M.S. and A.S.; validation, M.A.O., M.J.C., A.M.S. and A.S.; formal analysis, M.A.O., M.J.C., A.M.S. and A.S.; investigation, M.A.O., M.J.C., A.M.S. and A.S.; resources, M.A.O., M.J.C., A.M.S. and A.S.; data curation, M.A.O., M.J.C., A.M.S. and A.S.; writing—original draft preparation, M.A.O., M.J.C., A.M.S. and A.S.; writing—review and editing, M.A.O., M.J.C., A.M.S. and A.S.; visualization, M.A.O., M.J.C., A.M.S. and A.S.; supervision, M.J.C., A.M.S. and A.S.; project administration, M.J.C. and A.S.; funding acquisition, M.J.C., A.M.S. and A.S.Y.Y. All authors have read and agreed to the published version of the manuscript.

Funding: This work was partially supported by FCT (Fundação para a Ciência e a Tecnologia) through the grant SFRH/BPD/86498/2012 with national funding. The work is co-funded by the European Union through the European Regional Development Fund, included in the COMPETE 2020 (Operational Program Competitiveness and Internationalization) through the ICT project (UIDB/04683/2020) with the reference POCL-01-0145-FEDER-007690 and also through TOMAQAPA (PTDC/CTAMET/ 29678/2017) and CILIFO (0753_CILIFO_5_E) projects. The work has been also partially funded by FEDER/Ministerio de Ciencia, Innovación y Universidades-Agencia Estatal de Investigación through project RTI 2018-097332-8-C22, and by Junta de Extremadura-FEDER through project GR18097.

Acknowledgments: The authors thank NASA Langley Research Center Atmospheric Sciences Data Center for the data provided to carry out this work.

Conflicts of Interest: The authors declare no conflict of interest

References

1. Sanchez-Lorenzo, A.; Calbó, J.; Brunetti, M.; Deser, C. Dimming/brightening over the Iberian Peninsula: Trends in sunshine duration and cloud cover and their relations with atmospheric circulation. *J. Geophys. Res. Space Phys.* **2009**, *114*, D00D09. [[CrossRef](#)]
2. Wild, M.; Folini, D.; Schär, C.; Loeb, N.; Dutton, E.G.; König-Langlo, G. The global energy balance from a surface perspective. *Clim. Dyn.* **2012**, *40*, 3107–3134. [[CrossRef](#)]
3. Wild, M.; Liepert, B. The Earth radiation balance as driver of the global hydrological cycle. *Environ. Res. Lett.* **2010**, *5*, 025203. [[CrossRef](#)]
4. Giorgi, F. Climate change hot-spots. *Geophys. Res. Lett.* **2006**, *33*. [[CrossRef](#)]

5. Papadimas, C.D.; Hatzianastassiou, N.; Mihalopoulos, N.; Querol, X.; Vardavas, I. Spatial and temporal variability in aerosol properties over the Mediterranean basin based on 6-year (2000–2006) MODIS data. *J. Geophys. Res. Space Phys.* **2008**, *113*. [[CrossRef](#)]
6. Lelieveld, J.; Berresheim, H.; Borrmann, S.; Crutzen, P.; Dentener, F.; Fischer, H.; Feichter, J.; Flatau, P.J.; Heland, J.; Holzinger, R.; et al. Global Air Pollution Crossroads over the Mediterranean. *Science* **2002**, *298*, 794–799. [[CrossRef](#)]
7. Formenti, P.; Andreae, M.O.; Andreae, T.W.; Galani, E.; Vasaras, A.; Zerefos, C.; Amiridis, V.; Orlovsky, L.; Karnieli, A.; Wendisch, M.; et al. Aerosol optical properties and large-scale transport of air masses: Observations at a coastal and a semiarid site in the eastern Mediterranean during summer 1998. *J. Geophys. Res. Space Phys.* **2001**, *106*, 9807–9826. [[CrossRef](#)]
8. Andreae, M.O.; Ichoku, C.; Cafmeyer, J.; Maenhaut, W.; Karnieli, A.; Orlovsky, L. Light scattering by dust and anthropogenic aerosol at a remote site in the Negev desert, Israel. *J. Geophys. Res. Space Phys.* **2002**, *107*, 107. [[CrossRef](#)]
9. Costa, M.J.; Sohn, B.-J.; Levizzani, V.; Silva, A.M. Radiative Forcing of Asian Dust Determined from the Synergized GOME and GMS Satellite Data—A Case Study. *J. Meteorol. Soc. Jpn.* **2006**, *84*, 85–95. [[CrossRef](#)]
10. Di Sarra, A.; Pace, G.; Meloni, D.; De Silvestri, L.; Piacentino, S.; Monteleone, F. Surface shortwave radiative forcing of different aerosol types in the central Mediterranean. *Geophys. Res. Lett.* **2008**, *35*, 02714. [[CrossRef](#)]
11. Santos, D.; Costa, M.J.; Silva, A.M. Direct SW aerosol radiative forcing over Portugal. *Atmos. Chem. Phys. Discuss.* **2008**, *8*, 5771–5786. [[CrossRef](#)]
12. Esteve, A.; Estelles, V.; Utrillas, M.P.; Martinez-Lozano, J.A. Analysis of the aerosol radiative forcing over a Mediterranean urban coastal site. *Atmos. Res.* **2014**, *137*, 195–204. [[CrossRef](#)]
13. Mateos, D.; Anton, M.; Toledano, C.; Cachorro, V.E.; Alados-Arboledas, L.; Sorribas, M.; Costa, M.J.; Baldasano, J.M. Aerosol radiative effects in the ultraviolet, visible, and near-infrared spectral ranges using long-term aerosol data series over the Iberian Peninsula. *Atmos. Chem. Phys. Discuss.* **2014**, *14*, 13497–13514. [[CrossRef](#)]
14. Obregón, M.A.; Pereira, S.N.; Salgueiro, V.; Costa, M.J.; Silva, A.M.; Serrano, A.; Bortoli, D. Aerosol radiative effects during two desert dust events in August 2012 over the Southwestern Iberian Peninsula. *Atmos. Res.* **2015**, *153*, 404–415. [[CrossRef](#)]
15. Obregón, M.A.; Costa, M.J.; Serrano, A.; Silva, A.M. Effect of water vapor in the SW and LW downward irradiance at the surface during a day with low aerosol load. *IOP Conf. Series: Earth Environ. Sci.* **2015**, *28*, 12009. [[CrossRef](#)]
16. Floutsi, A.A.; Korras-Carraca, M.B.; Matsoukas, C.; Hatzianastassiou, N.; Biskos, G. Climatology and trends of aerosol optical depth over the Mediterranean basin during the last 12 years (2002–2014) based on Collection 006 MODIS-Aqua data. *Sci. Total Environ.* **2016**, *551–552*, 292–303. [[CrossRef](#)]
17. Obregón, M.A.; Costa, M.J.; Silva, A.M.; Serrano, A. Thirteen Years of Aerosol Radiative Forcing in Southwestern Iberian Peninsula. *Aerosol Air Qual. Res.* **2017**, *17*, 2509–2521. [[CrossRef](#)]
18. Vaquero-Martínez, J.; Antón, M.; Ortiz-De-Galisteo, J.P.; Román, R.; Cachorro, V. Water vapor radiative effects on short-wave radiation in Spain. *Atmos. Res.* **2018**, *205*, 18–25. [[CrossRef](#)]
19. Trenberth, K.E.; Fasullo, J.T.; Smith, L. Trends and variability in column-integrated atmospheric water vapor. *Clim. Dyn.* **2005**, *24*, 741–758. [[CrossRef](#)]
20. Mattar, C.; Sobrino, J.A.; Julien, Y.; Morales, L. Trends in column integrated water vapour over Europe from 1973 to 2003. *Int. J. Clim.* **2010**, *31*, 1749–1757. [[CrossRef](#)]
21. Sorribas, M.; Andrews, E.; Ogren, J.; Del Águila, A.; Fraile, R.; Sheridan, P.; Yela, M. Climatological study for understanding the aerosol radiative effects at southwest Atlantic coast of Europe. *Atmos. Environ.* **2019**, *205*, 52–66. [[CrossRef](#)]
22. Mateos, D.; Antón, M.; Sanchez-Lorenzo, A.; Calbó, J.; Wild, M. Long-term changes in the radiative effects of aerosols and clouds in a mid-latitude region (1985–2010). *Glob. Planet. Chang.* **2013**, *111*, 288–295. [[CrossRef](#)]
23. Obregón, M.A.; Costa, M.J.; Silva, A.; Serrano, A. Impact of aerosol and water vapour on SW radiation at the surface: Sensitivity study and applications. *Atmos. Res.* **2018**, *213*, 252–263. [[CrossRef](#)]
24. Nabat, P.; Somot, S.; Mallet, M.; Chiapello, I.; Morcrette, J.J.; Solmon, F.; Szopa, S.; Dulac, F.; Collins, W.; Ghan, S.; et al. A 4-D climatology (1979–2009) of the monthly tropospheric aerosol optical depth distribution over the Mediterranean region from a comparative evaluation and blending of remote sensing and model products. *Atmos. Meas. Tech.* **2013**, *6*, 1287–1314. [[CrossRef](#)]

25. Alexandri, G.; Georgoulas, A.; Meleti, C.; Balis, D.; Kourtidis, K.; Sanchez-Lorenzo, A.; Trentmann, J.; Zanis, P. A high resolution satellite view of surface solar radiation over the climatically sensitive region of Eastern Mediterranean. *Atmos. Res.* **2017**, *188*, 107–121. [[CrossRef](#)]
26. Provençal, S.; Kishcha, P.; Da Silva, A.M.; Elhacham, E.; Alpert, P. AOD distributions and trends of major aerosol species over a selection of the world's most populated cities based on the 1st version of NASA's MERRA Aerosol Reanalysis. *Urban Clim.* **2017**, *20*, 168–191. [[CrossRef](#)]
27. Ho, S.-P.; Peng, L.; Mears, C.; Anthes, R.A. Comparison of global observations and trends of total precipitable water derived from microwave radiometers and COSMIC radio occultation from 2006 to 2013. *Atmos. Chem. Phys. Discuss.* **2018**, *18*, 259–274. [[CrossRef](#)]
28. Bilbao, J.; Román, R.; Yousif, C.; Mateos, D.; De Miguel, A. Total ozone column, water vapour and aerosol effects on erythemal and global solar irradiance in Marsaxlokk, Malta. *Atmos. Environ.* **2014**, *99*, 508–518. [[CrossRef](#)]
29. Goto, D.; Schutgens, N.A.J.; Nakajima, T.; Takemura, T. Sensitivity of aerosol to assumed optical properties over Asia using a global aerosol model and AERONET. *Geophys. Res. Lett.* **2011**, *38*, 17810. [[CrossRef](#)]
30. Wielicki, B.A.; Barkstrom, B.R.; Harrison, E.F.; Lee, R.B.; Smith, G.L.; Cooper, J.E. Clouds and the Earth's Radiant Energy System (CERES): An Earth Observing System Experiment. *Bull. Am. Meteorol. Soc.* **1996**, *77*, 853–868. [[CrossRef](#)]
31. Doelling, D.; Loeb, N.G.; Keyes, D.F.; Nordeen, M.L.; Morstad, D.; Nguyen, C.; Wielicki, B.; Young, D.F.; Sun, M. Geostationary Enhanced Temporal Interpolation for CERES Flux Products. *J. Atmos. Ocean. Technol.* **2013**, *30*, 1072–1090. [[CrossRef](#)]
32. Rutan, D.A.; Kato, S.; Doelling, D.; Rose, F.G.; Nguyen, L.T.; Caldwell, T.E.; Loeb, N.G. CERES Synoptic Product: Methodology and Validation of Surface Radiant Flux. *J. Atmos. Ocean. Technol.* **2015**, *32*, 1121–1143. [[CrossRef](#)]
33. Remer, L.A.; Kaufman, Y.J.; Tanré, D.; Mattoo, S.; Chu, D.A.; Martins, J.V.; Li, R.-R.; Ichoku, C.; Levy, R.C.; Kleidman, R.G.; et al. The MODIS Aerosol Algorithm, Products and Validation. *J. Atmos. Sci.* **2003**, *62*, 947–973. [[CrossRef](#)]
34. Collins, W.; Rasch, P.J.; Eaton, B.E.; Khattatov, B.V.; Lamarque, J.-F.; Zender, C. Simulating aerosols using a chemical transport model with assimilation of satellite aerosol retrievals: Methodology for INDOEX. *J. Geophys. Res. Space Phys.* **2001**, *106*, 7313–7336. [[CrossRef](#)]
35. Gao, B.-C.; Kaufman, Y.J. Water vapor retrievals using Moderate Resolution Imaging Spectroradiometer (MODIS) near-infrared channels. *J. Geophys. Res. Space Phys.* **2003**, *108*, 4389. [[CrossRef](#)]
36. Sayer, A.M.; Hsu, N.C.; Bettenhausen, C.; Jeong, M.-J. Validation and uncertainty estimates for MODIS Collection 6 “Deep Blue” aerosol data. *J. Geophys. Res. Atmos.* **2013**, *118*, 7864–7872. [[CrossRef](#)]
37. Chu, D.A.; Kaufman, Y.J.; Ichoku, C.; Remer, L.A.; Tanré, D.; Holben, B.N. Validation of MODIS aerosol optical depth retrieval over land. *Geophys. Res. Lett.* **2002**, *29*, 1617. [[CrossRef](#)]
38. Mishra, A.K.; Rudich, Y.; Koren, I. Spatial boundaries of Aerosol Robotic Network observations over the Mediterranean basin. *Geophys. Res. Lett.* **2016**, *43*, 2259–2266. [[CrossRef](#)]
39. Prasad, A.; Singh, R.P. Validation of MODIS Terra, AIRS, NCEP/DOE AMIP-II Reanalysis-2, and AERONET Sun photometer derived integrated precipitable water vapor using ground-based GPS receivers over India. *J. Geophys. Res. Space Phys.* **2009**, *114*. [[CrossRef](#)]
40. Sen, P.K. Estimates of the regression coefficient based on Kendall's tau. *J. Amer. Stat. Assoc.* **1968**, *63*, 1379–1389. [[CrossRef](#)]
41. Estelles, V.; Martinez-Lozano, J.A.; Utrillas, M.P. Influence of air mass history on the columnar aerosol properties at Valencia, Spain. *J. Geophys. Res. Space Phys.* **2007**, *112*, 112. [[CrossRef](#)]
42. Lyamani, H.; Olmo, F.; Alados-Arboledas, L. Physical and optical properties of aerosols over an urban location in Spain: Seasonal and diurnal variability. *Atmos. Chem. Phys. Discuss.* **2010**, *10*, 239–254. [[CrossRef](#)]
43. Pereira, S.N.; Wagner, F.; Silva, A.M. Seven years of measurements of aerosol scattering properties, near the surface, in the southwestern Iberia Peninsula. *Atmos. Chem. Phys. Discuss.* **2011**, *11*, 17–29. [[CrossRef](#)]
44. Obregón, M.A.; Pereira, S.N.; Wagner, F.; Serrano, A.; Cancillo, M.L.; Silva, A.M. Regional differences of column aerosol parameters in western Iberian Peninsula. *Atmos. Environ.* **2012**, *62*, 208–219. [[CrossRef](#)]
45. Evgenieva, T.T.; Wiman, B.L.B.; Kolev, N.I.; Savov, P.B.; Donev, E.H.; Ivanov, D.I.; Danchovski, V.; Kaprielov, B.K.; Grigorieva, V.N.; Iliev, I.; et al. Three-point observation in the troposphere over Sofia-Plana Mountain, Bulgaria. *Int. J. Remote Sens.* **2011**, *32*, 9343–9363. [[CrossRef](#)]

46. Papadimas, C.D.; Hatzianastassiou, N.; Matsoukas, C.; Kanakidou, M.; Mihalopoulos, N.; Vardavas, I. The direct effect of aerosols on solar radiation over the broader Mediterranean basin. *Atmos. Chem. Phys. Discuss.* **2012**, *12*, 7165–7185. [CrossRef]
47. Schepanski, K.; Tegen, I.; Todd, M.C.; Heinold, B.; Bonisch, G.; Laurent, B.; Macke, A. Meteorological processes forcing Saharan dust emission inferred from MSG-SEVIRI observations of subdaily dust source activation and numerical models. *J. Geophys. Res. Space Phys.* **2009**, *114*. [CrossRef]
48. Malico, I.; Pereira, S.N.; Costa, M.J. Black carbon trends in southwestern Iberia in the context of the financial and economic crisis. The role of bioenergy. *Environ. Sci. Pollut. Res.* **2016**, *24*, 476–488. [CrossRef]
49. Chiapello, I.; Bergametti, G.; Gomes, L.; Chatenet, B.; Dulac, F.; Pimenta, J.; Soares, E.S. An additional low layer transport of Sahelian and Saharan dust over the north-eastern Tropical Atlantic. *Geophys. Res. Lett.* **1995**, *22*, 3191–3194. [CrossRef]
50. Díaz, A.M.; Díaz, J.P.; Exposito, F.J.; Hernández-Leal, P.A.; Savoie, D.; Querol, X. Air masses and aerosols chemical components in the free troposphere at the subtropical northeast atlantic region. *J. Atmos. Chem.* **2006**, *53*, 63–90. [CrossRef]
51. Palau, J.L.; Rovira, F.; Sales, M.J. Satellite Observations of the Seasonal Evolution of Total Precipitable Water Vapour over the Mediterranean Sea. *Adv. Meteorol.* **2017**, *2017*, 1–9. [CrossRef]
52. Millán, M.M.; Mantilla, E.; Salvador, R.; Kallos, G. Photooxidant dynamics in the Mediterranean basin in summer: Results from European research projects. *J. Geophys. Res. Space Phys.* **1997**, *102*, 8811–8823. [CrossRef]
53. Levy, I.; Dayan, U.; Mahrer, Y. A five-year study of coastal recirculation and its effect on air pollutants over the East Mediterranean region. *J. Geophys. Res. Space Phys.* **2008**, *113*, 113. [CrossRef]
54. Kallos, G.; Mitsakou, C.; Alastuey, A. Mechanisms of climate variability, air quality and impacts of atmospheric constituents in the Mediterranean Region. In *Regional Assessment Climate Change in the Mediterranean*; Navarra, A., Tubiana, L., Eds.; Springer: Berlin, Germany, 2013; Volume 3, pp. 119–156.
55. Millán, M.M.; Estrela, M.J.; Sanz, M.J.; Mantilla, E.; Martin, M.; Pastor, F.; Salvador, R.; Vallejo, V.R.; Alonso, L.; Gangoiti, G.; et al. Climatic Feedbacks and Desertification: The Mediterranean Model. *J. Clim.* **2005**, *18*, 684–701. [CrossRef]
56. Hoegh-Guldberg, O.; Jacob, D.; Taylor, M.; Bindi, M.; Brown, S.; Camilloni, I.; Diedhiou, A.; Djalante, R.; Ebi, K.L.; Engelbrecht, F.; et al. Impacts of 1.5 °C Global Warming on Natural and Human Systems. In *Global Warming of 1.5 °C. An IPCC Special Report on the Impacts of Global Warming of 1.5 °C Above Pre-Industrial Levels and Related Global Greenhouse Gas Emission Pathways, in the Context of Strengthening the Global Response to the Threat of Climate Change, Sustainable Development, and Efforts to Eradicate Poverty*; Masson-Delmotte, V., Zhai, P., Pörtner, H.-O., Roberts, D., Skea, J., Shukla, P.R., Pirani, A., Moufouma-Okia, W., Péan, C., Pidcock, R., Eds.; World Meteorological Organization Technical Document; IPCC Secretariat: Geneva, Switzerland, 2018; in press.
57. Santacatalina, M.; Yubero, E.; Mantilla, E.; Carratalá, A. Relevance of the economic crisis in chemical PM10 changes in a semi-arid industrial environment. *Environ. Monit. Assess.* **2011**, *184*, 6827–6844. [CrossRef] [PubMed]
58. Monteiro, A.; Russo, M.; Gama, C.; Lopes, M.; Borrego, C. How economic crisis influence air quality over Portugal (Lisbon and Porto)? *Atmos. Pollut. Res.* **2018**, *9*, 439–445. [CrossRef]
59. Eurostat, *Eurostat Review on National Accounts and Macroeconomic Indicators*; 2016; ISSN 2443–7832. Available online: <http://ec.europa.eu/eurostat/documents/3217494/7784358/KS-GP-16-002-EN-N.pdf> (accessed on 17 April 2020).
60. Collins, M.; Knutti, R.; Arblaster, J.; Dufresne, J.L.; Fichefet, T.; Friedlingstein, P.; Gao, X.; Gutowski, W.J.; Johns, T.; Krinner, G.; et al. Long-term Climate Change: Projections, Commitments and Irreversibility. In *Climate Change 2013: The Physical Science Basis. Contribution of Working Group I to the Fifth Assessment Report of the Intergovernmental Panel on Climate Change*; Stocker, T.F., Qin, D., Plattner, G.-K., Tignor, M., Allen, S.K., Boschung, J., Nauels, A., Xia, Y., Bex, V., Midgley, P.M., Eds.; Cambridge University Press: Cambridge, UK; New York, NY, USA, 2013.
61. Zhang, J.; Reid, J.S. A decadal regional and global trend analysis of the aerosol optical depth using a data-assimilation grade over-water MODIS and Level 2 MISR aerosol products. *Atmos. Chem. Phys. Discuss.* **2010**, *10*, 10949–10963. [CrossRef]

62. Alfaro-Contreras, R.; Zhang, J.; Reid, J.S.; Christopher, S. A study of 15-year aerosol optical thickness and direct shortwave aerosol radiative effect trends using MODIS, MISR, CALIOP and CERES. *Atmos. Chem. Phys. Discuss.* **2017**, *17*, 13849–13868. [[CrossRef](#)]
63. Alam, K.; Trautmann, T.; Blaschke, T.; Subhan, F. Changes in aerosol optical properties due to dust storms in the Middle East and Southwest Asia. *Remote. Sens. Environ.* **2014**, *143*, 216–227. [[CrossRef](#)]
64. Shalaby, A.; Rappenglueck, B.; Eltahir, E.A.B. The climatology of dust aerosol over the arabian peninsula. *Atmos. Chem. Phys. Discuss.* **2015**, *15*, 1523–1571. [[CrossRef](#)]
65. Gharibzadeh, M.; Alam, K.; Bidokhti, A.A.; Abedini, Y.A.Y.; Masoumi, A. Radiative Effects and Optical Properties of Aerosol during Two Dust Events in 2013 over Zanzan, Iran. *Aerosol Air Qual. Res.* **2017**, *17*, 888–898. [[CrossRef](#)]
66. Chen, B.; Liuid, Z. Global water vapor variability and trend from the latest 36 year (1979 to 2014) data of ECMWF and NCEP reanalyses, radiosonde, GPS, and microwave satellite. *J. Geophys. Res. Atmos.* **2016**, *121*, 1144–11462. [[CrossRef](#)]
67. Zhang, Y.H.; Xu, J.; Yang, N.; Lan, P. Variability and Trends in Global Precipitable Water Vapor Retrieved from COSMIC Radio Occultation and Radiosonde Observations. *Atmosphere* **2018**, *9*, 174. [[CrossRef](#)]
68. Ciardini, V.; Contessa, G.M.; Falsaperla, R.; Gómez-Amo, J.L.; Meloni, D.; Monteleone, F.; Pace, G.; Piacentino, S.; Sferlazzo, D.; Di Sarra, A. Global and Mediterranean climate change: A short summary. *Ann. Ist. Super. Sanita* **2016**, *52*, 325–337. [[PubMed](#)]
69. Gurbuz, G.; Jin, S. Long-time variations of precipitable water vapour estimated from GPS, MODIS and radiosonde observations in Turkey. *Int. J. Clim.* **2017**, *37*, 5170–5180. [[CrossRef](#)]



© 2020 by the authors. Licensee MDPI, Basel, Switzerland. This article is an open access article distributed under the terms and conditions of the Creative Commons Attribution (CC BY) license (<http://creativecommons.org/licenses/by/4.0/>).